Direct Observation of Redox-Linked Histidine Protonation Changes in the Iron−Sulfur Protein of the Cytochrome bc_1 Complex by ATR-FTIR Spectroscopy[†]

Masayo Iwaki,[‡] Gregory Yakovlev,[§] Judy Hirst,[§] Artur Osyczka,[||] P. Leslie Dutton,[||] Douglas Marshall,[‡] and Peter R. Rich*[,‡]

Glynn Laboratory of Bioenergetics, Department of Biology, University College London, Gower Street, London WC1E 6BT, U.K., Medical Research Council Dunn Human Nutrition Unit, Wellcome Trust/MRC Building, Hills Road, Cambridge CB2 2XY, U.K., and The Johnson Research Foundation, Department of Biochemistry and Biophysics, University of Pennsylvania, 1004 Stellar-Chance Building, 422 Curie Boulevard, Philadelphia, Pennsylvania 19104

Received November 23, 2004; Revised Manuscript Received January 14, 2005

ABSTRACT: The redox-linked protonation chemistry of the iron−sulfur protein (ISP) of the cytochrome bc_1 complex was studied by analysis of the pH dependencies of redox difference spectra using perfusion/electrochemically induced attenuated total reflection-Fourier transform infrared (ATR-FTIR) spectroscopy. The ISP of *Rhodobacter capsulatus* within the intact cytochrome bc_1 complex was analyzed in a mutant form in which the midpoint potential of cytochrome c_1 was lower than that of the ISP. This was compared to a soluble domain of the ISP from the bovine bc_1 complex. Spectra of in situ bacterial and isolated bovine proteins differ markedly only in part of their amide I regions with the in situ protein having additional pH-dependent component(s). Apart from this, both in situ and isolated proteins exhibited the same pH-dependent IR features in reduced minus oxidized difference spectra. Specifically, at high pH, a strong H/D insensitive negative band appeared at 1447/1450 cm^{-1}, together with a peak at 1310 cm^{-1}, the change of a 1267/1255 cm^{-1} peak/trough into a simple 1266 cm^{-1} peak, and a trough at 1107 cm^{-1}. Comparison with spectra of model materials indicates that all four signals arise from an imidazolate to imidazole transition of histidine, hence providing the first direct demonstration that histidine is the redox-linked protonation site of the ISP. The 1450 cm^{-1} band can be assigned to a ring stretch that is unique to the imidazolate form of histidine. It is relatively sharp, has a high extinction coefficient, and provides a novel marker band for the detection of imidazolate intermediates in enzymatic mechanisms generally.

The cytochrome bc_1 complex forms a superfamily of membrane-embedded enzymes that occur widely in eukaryotic and prokaryotic respiratory and photosynthetic electron transfer chains. A common core complex encoded by *pet* genes consists of three subunits: the "Rieske" iron−sulfur protein (ISP),[1] cytochrome c_1, and cytochrome *b*. These contain a [2Fe-2S] cluster, heme C, and two heme B molecules, respectively. The core catalyzes ubiquinol-cytochrome *c* oxidoreductase and associated transmembrane proton transfer activities. Structures of eukaryotic and bacterial *bc* complexes and of the homologous cytochrome *bf* complex from cyanobacteria and green algae have been determined at atomic resolution (*1*−*7*). It is widely agreed that electron and proton transfer occur by a "Q-cycle" mechanism (*8*). Ubiquinol is oxidized at the "Q_o" site by a mechanism in which one electron is transferred to the ISP and the other to the lower-potential heme b_L. The chemical and physical factors that cause this unusual chemistry at the Q_o site have remained controversial. For example, questions of whether a remarkable long-range rotation of the globular domain of the ISP center is an essential feature for bifurcated electron transfer remain (*9*−*12*). On the basis of positions of various bound inhibitors, the Q_o site appears to be rather extensive such that two sequential binding positions for ubiquinone species might be operative (*13*). Several other studies indicate that two ubiquinones may be bound simultaneously within the Q_o site (*14*−*17*). These complications have led to a range of mechanistic models (*10*, *11*, *13*, *17*−*22*). However, a recent detailed quantitative assessment based upon predicted electron transfer rates (*23*) has led to the conclusion that none can satisfactorily account for the rapid reversibility and low rates of unwanted "leak" reactions. It was concluded that this could be achieved only by a "true" concerted $n = 2$ oxidation of quinol or by addition of further complicating gating mechanisms (*23*), several possibilities of which were outlined subsequently (*13*, *24*−*27*). Testing of these models requires knowledge of structure of the enzyme−substrate complex and of the groups within the protein that are specifically responsible for the extensive redox-linked protonation changes that are integral to the catalytic cycle. Transmission- and attenuated total reflection (*28*) (ATR)-Fourier transform infrared (FTIR) spectroscopy offer an experimental

[†] This work was funded by grants from the Wellcome Trust (Grant 062827) to P.R.R., the Medical Research Council to J.H., and the U.S. Public Health Service (Grant GM-27309) to P.L.D.

* To whom correspondence should be addressed: Glynn Laboratory of Bioenergetics, Department of Biology, University College London, Gower Street, London WC1E 6BT, U.K. Telephone and fax: (+44) 020 7679 7746. E-mail: prr@ucl.ac.uk.

[‡] University College London.

[§] Medical Research Council Dunn Human Nutrition Unit.

[||] University of Pennsylvania.

[1] Abbreviations: ATR-FTIR, attenuated total reflection-Fourier transform infrared; ISP, Rieske iron−sulfur protein.

10.1021/bi047533v CCC: $30.25
Published on Web 02/18/2005

probe, with successful applications to diverse proteins such as rhodopsin and bacteriorhodopsin (*29*), the nicotinic acetylcholine receptor (*30*), photosynthetic reaction centers (*31*−*33*), cytochrome *c* oxidase (*34*−*42*), complex I (*43*), and the bc_1 complex (*44*−*47*). In these latter reports, reduced minus oxidized IR difference spectra of the ISP have been reported. The ISP is thought to bind to substrate ubiquinol in the Q_o site through one of its metal-ligated histidine ligands (*2*, *4*, *24*, *27*, *48*), and one or both of these histidines are widely believed to provide the redox-linked protonation sites (*49*, *50*). In this report, we use IR spectroscopy to demonstrate directly that histidine does indeed undergo a redox-linked imidazolate−imidazole transition and report an IR marker band around 1450 cm^{-1} that may be used to detect the participation of imidazolate in enzymatic reactions more generally.

MATERIALS AND METHODS

Sample Preparation. Wild-type and mutant forms of the cytochrome bc_1 complex were isolated and purified from *Rhodobacter capsulatus* as described in ref *51*. The *Rba. capsulatus* strain containing the M183K mutation was a generous gift from F. Daldal. Generation and properties of this mutant have been described in ref *52*.

The soluble domain of the Rieske protein from the bovine bc_1 complex (comprising residue 70 to the C-terminus) was overexpressed in *Escherichia coli* as a holoprotein with a six-histidine tag on the N-terminus and purified as described in ref *53*.

Perfusion ATR-FTIR Spectroscopy. The production, manipulation, and ATR-FTIR analysis of films of the detergent-depleted cytochrome bc_1 complex from *Rba. capsulatus* were identical to those described in ref *47*. Perfusion buffers were either 10 mM 2-(*N*-morpholino)ethanesulfonic acid (MES), 50 mM potassium phosphate, 100 mM KCl, and 50 mM K_2SO_4 (pH 6 or 6.5) or 10 mM 2-(*N*-cyclohexylamino)-ethanesulfonic acid (CHES), 100 mM potassium phosphate, 100 mM KCl, and 50 mM K_2SO_4 (pH 9). Redox changes of ISP were induced by switching between buffers containing either 100 μM hydroquinone and 1 mM ferrocyanide or 1 mM ferricyanide. IR spectra were recorded at room temperature with a Bruker IFS 66S spectrometer equipped with a liquid nitrogen-cooled MCT-A detector and a silicon ATR microprism (3 mm diameter; three reflections; SensIR Europe) as described in ref *28*. For each transition, a background spectrum was recorded (500 interferograms over the course of 60 s), buffer was changed, and an equivalent sample spectrum was recorded 30 s after exchanging the buffer. Redox difference spectra that are shown are averages of batches of reduced minus oxidized and inverted oxidized minus reduced difference spectra. Corrections were made where necessary for any baseline drift due to protein swelling or shrinkage. IR spectra were measured with a resolution of 4 cm^{-1} and have an accuracy of ± 1 cm^{-1}.

Electrochemically Induced ATR-FTIR Spectroscopy. An electrochemical device was constructed in-house (Figure 1) that allowed automated redox manipulation of the soluble ISP domain in conjunction with ATR-FTIR measurements. A 9 mm diameter glassy carbon working electrode was placed approximately 0.2 mm above the ATR prism and formed the top of a sample chamber with a volume of approximately 20 μL. The chamber was connected via a Vycor salt bridge to a platinum spade counter electrode and a silver/silver chloride reference electrode. Computer-controlled voltage offset circuitry was used in conjunction with a PAR model 174A potentiostat to allow automated switching of the ambient potential of the sample mixture. The ISP sample was concentrated to approximately 3 mM in the appropriate buffer by ultrafiltration. Glycerol (2%, w/v) was then added as a stabilizer, together with 500 μM ferricyanide and 25 μM benzyl viologen as mediators. The buffer consisted of 25 mM *N*-(2-hydroxyethyl)piperazine-*N*′-2-ethanesulfonic acid (HEPES), 25 mM potassium phosphate, and 200 mM KCl (pH 7.2−8.0) or 25 mM CHES, 25 mM potassium phosphate, and 200 mM KCl (pH/pD 9.0−10.0). Each redox difference spectrum was obtained by recording a background spectrum (an average of 1000 interferograms over the course of 2 min) at one potential, switching the working electrode potential, and recording a sample spectrum (1000 interferograms) versus the background after redox equilibration. A new background was then recorded and the process repeated. The working potentials that were used were 550 and −350 mV versus SHE with 6 min allowed for redox equilibration. Redox difference spectra that are shown are averages of batches of reduced minus oxidized and inverted oxidized minus reduced difference spectra. Corrections were made where necessary for any baseline drift due to protein swelling or shrinkage.

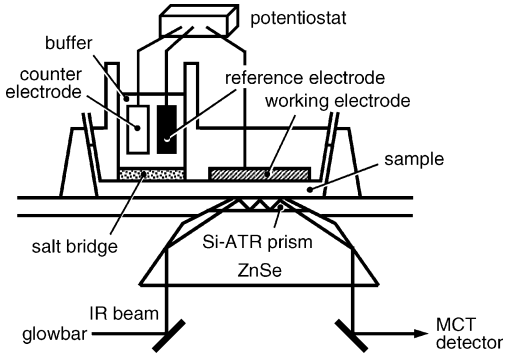

FIGURE 1: Combination electrochemical/ATR-FTIR spectroscopy device. The sample chamber is made of a nonconducting polymer, and the actual scale is not proportional to the drawing. See the text for details.

IR Spectra of Model Compounds. Absolute ATR-FTIR spectra of L-histidine and 4-methylimidazole were measured with the same ATR prism without a chamber for flow/electrochemistry. L-Histidine (Aldrich) and 4-methylimidazole (Aldrich) were dissolved to a concentration of 500 mM in distilled water or deuterium oxide (D_2O) to which NaOH had been added to provide the required pH/pD. A 100 μL aliquot of each sample solution was placed on the ATR microprism, and the absolute absorption spectra were recorded (each the average of 1000 interferograms). In all cases, spectra of solvent alone were recorded separately and subtracted from these spectra to produce the spectra that are shown. For extinction coefficient calculations, 10 mM potassium ferrocyanide was included and the frequency-dependent path length was calculated from its extinction coefficient of 4140 M^{-1} cm^{-1} at 2038 cm^{-1} (determined by transmission IR separately).

For measurements in D_2O, buffers prepared assuming pD $= pH_{reading} + 0.4$ (*54*) were substituted throughout the

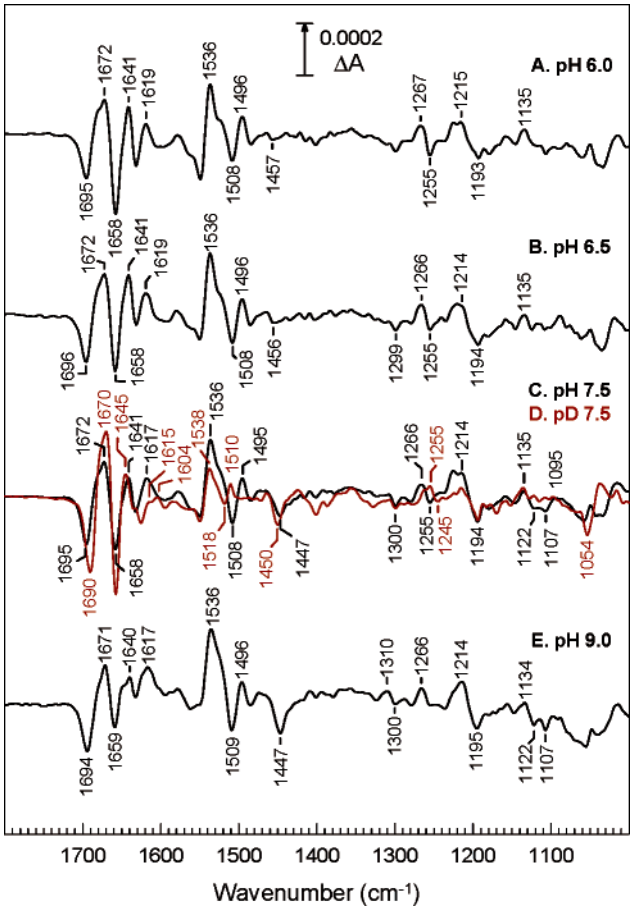

FIGURE 2: Perfusion-induced ATR-FTIR redox difference spectra of the ISP in the M183K mutant form of the *Rba. capsulatus* cytochrome bc_1 complex. Reduced minus oxidized IR difference spectra of the ISP at the indicated pH values are shown. Spectra A, B, and E are averages of 25, 21, and 42 reductive/oxidative cycles, respectively. The overlaid data at pH 7.5 (C, black) and pD 7.5 (D, red) were taken from ref *47*.

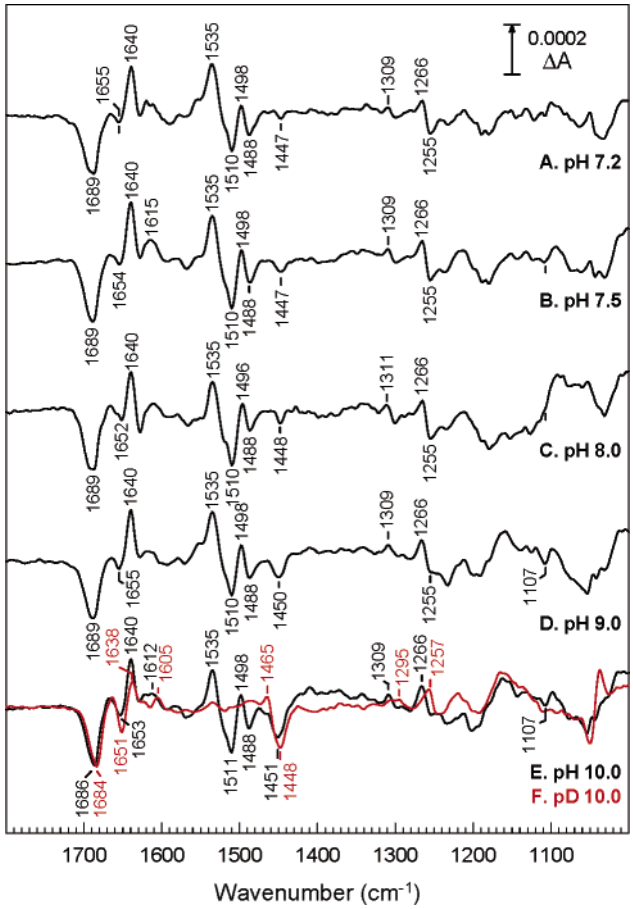

FIGURE 3: Electrochemically induced ATR-FTIR redox difference spectra of the globular domain of the bovine ISP. Reduced minus oxidized IR difference spectra of the ISP at the indicated pH values are shown, together with one after H−D exchange at pD 10 (trace F, red). Spectra A−F are averages of 3, 45, 57, 38, 34, and 30 reductive/oxidative cycles, respectively.

detergent depletion or concentrating procedures. The extent of H−D exchange in protein samples was estimated to be >90% using the method described in ref *55*.

RESULTS

Perfusion-Induced IR Difference Spectra of the Bacterial ISP in Situ. Redox transitions of the ISP in the intact bacterial bc_1 complex were induced by alternation of buffer containing 100 μM hydroquinone and 1 mM ferrocyanide with the same buffer containing 1 mM ferricyanide. In the M183K mutant enzyme, these reagents do not induce redox changes in cytochrome c_1 because of its lowered midpoint potential (*52*) and the resulting redox difference spectra therefore arise solely from the ISP. Redox difference spectra between pH 6 and 9 are shown in Figure 2. The pH/pD 7.5 data were published in ref *47* and are included here for comparison. Visible difference spectra in the 500−600 nm region, which were measured concurrently with FTIR measurement (*47*), confirmed that no redox changes in hemes B and C were occurring (data not shown). Major bands in H_2O media at all pH values occur at 1695(−), 1672(+), 1658(−), 1641(+), 1617(+), 1536(+), 1508(−), 1495(+), 1214(+), 1194(−), and 1135(+) cm^{-1} and are generally consistent with other published data (*44*, *45*, *47*). H−D exchange caused small shifts in the amide I region, though with a much larger than expected loss of the 1617 cm^{-1} peak, together with a large loss of signals in the amide II region. Several additional pH-dependent features were observed, the most prominent of which was the appearance at high pH of a trough at 1447 cm^{-1} and a trough at 1658 cm^{-1} that decreased in intensity at higher pH. Some smaller changes consisted of the appearance at high pH of a peak at 1310 cm^{-1}, the change of a 1267/1255 cm^{-1} peak trough into a simple 1266 cm^{-1} peak, and, barely discernible above noise but consistent with model data below, an increased trough at 1107 cm^{-1}. The effects of H−D exchange on the 1447 cm^{-1} band were obscured by an additional overlapping change in D_2O, presumably an amide II band that had shifted down into this region. However, it seems likely that the 1447 cm^{-1} trough was little affected by the H−D exchange itself. In contrast, H−D exchange caused a 9 cm^{-1} downshift of the 1266 cm^{-1} peak and a loss of the 1107 cm^{-1} trough. The signal-to-noise ratio was not high enough to assess the effect of H−D exchange on the 1310 cm^{-1} peak.

Electrochemically Induced IR Difference Spectra of the Soluble Bovine ISP Globular Domain. Figure 3 shows the reduced minus oxidized redox IR difference spectra of a fragment of the bovine ISP at pH values between 7.2 and 10. This fragment consists of the entire globular domain containing the [2Fe-2S] cluster and a part of the "hinge" region. At all pH values, major bands are evident at 1689-

(−), 1654(−), 1640(+), 1615(+), 1535(+), 1510(−), and 1498(+) cm^{-1}. This is in general agreement with published IR data on the fragment (*45*, *46*) but at a considerably higher signal-to-noise ratio. Again, several pH-dependent bands were evident, the most notable being the appearance at high pH of a trough at 1451 cm^{-1}, together with a small peak at 1310 cm^{-1}, the change of a 1266/1255 cm^{-1} peak/trough into a simple 1266 cm^{-1} peak, and a weak trough at 1107 cm^{-1}. H−D exchange caused only small shifts in the amide I region, although again with a large effect on the 1615 cm^{-1} peak, and much larger losses in the amide II region as expected. The trough at 1658 cm^{-1}, the intensity of which exhibited a strong pH dependence in the in situ bacterial ISP, was not seen in the spectra of the bovine ISP fragment. As was the case for the bacterial data given above, the effects of H−D exchange on the 1451 cm^{-1} band were obscured by an additional overlapping change in D_2O, presumably an amide II band that had shifted down into this region. However, it seems likely that the 1451 cm^{-1} trough was little affected by the H−D exchange itself. In contrast, H−D exchange caused a 9−14 cm^{-1} downshift of the 1310 and 1266 cm^{-1} peaks and a loss of the 1107 cm^{-1} trough. Reliable spectra at pH values lower than 7 could not be obtained because of protein instability.

It might be noted that, in this closed system electrochemistry mode, changes due to buffer protonation changes should appear in the redox IR difference spectra when the protein undergoes redox-dependent protonation changes. Indeed, separate control experiments at high pH (not shown) where the ISP has a redox-coupled protonated state change (Figure 3D−F) confirm that the broad apparent baseline variations at 1220(−)/1170(+) cm^{-1} in fact arise from deprotonation of CHES buffer and the peak around 1010 cm^{-1} arises from phosphate deprotonation. However, these buffer bands are broad in comparison to the underlying protein bands and occur in only these two regions. Hence, they do not interfere with the conclusions concerning protein-related bands.

DISCUSSION

Since vibrational modes of the [2Fe-2S] prosthetic group are expected only below 800 cm^{-1}, the changes reported in this study arise solely from protein vibrational modes. The major changes occur between 1695−1617 and 1536−1508 cm^{-1} and are likely to be dominated by amide I and amide II polypeptide backbone changes. This is supported in general by the H−D effects which affect amide I modes weakly ($\Delta\nu$ = −1 to −3 cm^{-1}) and amide II modes more strongly ($\Delta\nu$ = −20 to −40 cm^{-1}). In the redox spectra of the intact ISP, the prominent trough at 1695 cm^{-1} in the amide I region has been observed consistently (*5*, *44*−*47*). An amide I C═O stretching band at this frequency can be associated with backbone turns and bends (*56*), and it was suggested (*46*) that it could possibly be associated with changes in the conformation of the hinge region of the ISP that have been observed in crystallographically determined structures (*1*−*4*). However, the data on the isolated globular domain (Figure 2 and ref *45*) show a trough similar in magnitude, clearly ruling this out. In fact, comparison of the bacterial in situ and bovine fragment data (spectra at pH 7.5 are overlaid in Figure 4) shows that they are quite comparable across the 2000−1000 cm^{-1} region generally, differing only in a 1672/1658 cm^{-1} peak/trough that is very prominent in the in situ protein and essentially absent from the bovine fragment. It is possible that this arises from several components since the trough intensity was pH-dependent whereas the peak intensity was not, and might simply reflect a structural difference between bacterial and bovine proteins, particularly since the bacterial form has two additional insertions (*57*) that could affect both redox-linked structural changes and surface charge (*5*). However, IR data from other groups (*44*, *45*) also appear to show the same difference between the ISP in the intact bacterial *bc* complex and the equivalent bacterial fragment. Hence, if the stable position of the ISP globular domain is sensitive to its redox state, a point that is yet to be established, this bandshift difference should be analyzed further as a candidate in the amide I region for an IR change associated with the hinge region restructuring.

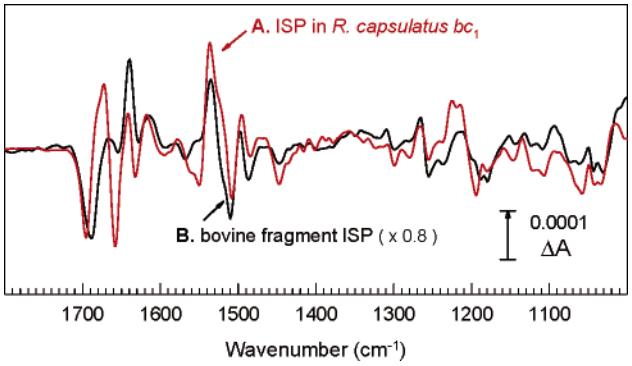

FIGURE 4: Comparison of bacterial ISP in situ and bovine ISP soluble domain spectra at pH 7.5. *Rba. capsulatus* data of Figure 2C (trace A, red) and bovine data of Figure 3B (trace B, black) are overlaid for the purposes of comparison.

As noted previously (*47*), the degree of H−D exchange sensitivity of the amide I region is somewhat greater than expected if the changes arise solely from amide I changes, particularly the band at 1617(+) cm^{-1}, which is rather outside the amide I envelope and is lost on H−D exchange. Hence, it seems likely that changes of H−D sensitive amino acids are also present within this region, possibly related to residues in the hydrogen bonding network of the cluster. Five hydrogen bonds from serine, tyrosine, and the backbone to the bovine cluster can be identified (*58*), and it has been suggested that the H-bonding network contracts on cluster reduction on the basis of reduction enthalpies (*59*). The imidazolate−imidazole transition of histidine (see below) may also contribute H−D sensitive bands within the amide I region.

The peak at 1536/1535 cm^{-1} is very sensitive to H−D exchange in both samples and is consistent with assignment predominantly to amide II shifts, as has been suggested for the *Rba. capsulatus* ISP (*44*) and an ISP fragment of *Paracoccus denitrificans* (*45*). Whereas in D_2O little remains in this region in the bovine fragment, a sharp peak/trough at 1510/1518 cm^{-1} is revealed in the bacterial ISP. Protonated tyrosine has an intense C═C band in this region, and a redox-linked environment change could give such a feature. Only two tyrosine residues are present in the *Rba. capsulatus* sequence, Y16 and Y160 (*Rba. capsulatus* numbering). However, Y16 is close to the end of the membrane-spanning region of the *Rba. capsulatus* ISP and on the opposite side of the membrane from the headgroup (*5*), and Y160 is present in the bovine ISP within a highly conserved region even

though the band is not evident in the bovine spectra. Hence, no clear assignment is possible without further studies of mutants at these positions.

Redox-Linked Protonation. This work was carried out primarily with the aim of establishing the sites of redox-linked protonation within the ISP that are known from potentiometric data to arise from two groups with p*K* values on the oxidized proteins of 7.6 and 9.2 in the globular domain of the bovine ISP (*49*) [7.6 and 9.8, respectively, in *Rhdodbacter sphaeroides* ISP (*57*)]. Mechanistic, structural, and computational data have suggested that the lower p*K* and, possibly, the higher p*K* are associated with the histidine ligands to the iron−sulfur cluster (*57*, *58*, *60*). Indirect support for this has been provided by Mössbauer (*61*), resonance Raman (*60*, *62*), and ESEEM (*63*) spectroscopies, but direct confirmation has been lacking.

The most prominent effect of pH was on the trough at 1447 cm^{-1}. A similar trough is seen in the corresponding spectrum of the *Rba. capsulatus* enzyme and was assigned tentatively to a ring vibration of proline (P140 and/or P170, *Rba. capsulatus* numbering) or tryptophan (*44*). W151 would be approximately 10 Å from the metal center if its position is equivalent to that of W176 in the yeast ISP sequence (*4*). However, this residue is replaced by Y156 in the bovine ISP. Hence, neither tryptophan nor proline, which is not protonatable, is likely to cause this band. Hasegawa et al. (*64*) studied the Raman and IR properties of 4-methylimidazole as a model for histidine, and it is clear from their data that the imidazolate form of this compound has a particularly strong vibration at 1440 cm^{-1} arising in part from ring CN stretch, which is lost upon protonation. This is shown clearly in Figure 5, especially in the calculated 4-methylimidazole minus 4-methylimidazolate difference spectrum where a sharp trough at 1438 cm^{-1} is apparent. The IR spectra of the equivalent imidazole and imidazolate forms of L-histidine, together with calculated imidazole minus imidazolate difference spectra, are shown in Figure 6. The absolute spectra are sufficiently similar to the 4-methylimidazole data of Hasegawa et al. (*64*, *65*) that their calculated assignments, together with more limited data on histidine itself (*66*), can provide a solid interpretation of the L-histidine bands. An equivalent of the 4-methylimidazolate 1440 cm^{-1} band is found at 1451 cm^{-1} in the imidazolate form of L-histidine, and this results in a prominent trough in the difference spectrum. Two further notable positive bands are seen at 1323 and 1262 cm^{-1}, together with a trough at 1102 cm^{-1}. Whereas the 1451 and 1102 cm^{-1} bands are relatively H−D exchange insensitive, the 1323 and 1262 cm^{-1} bands are both downshifted by 5−10 cm^{-1}. Equivalents of these are evident in the high-pH redox spectra of the ISP (Figures 2 and 3) at 1447−1451, 1310, 1266, and 1107 cm^{-1}. Furthermore, the H−D insensitivity of the 1447−1451 cm^{-1} band and the H−D exchange-induced downshifts of the 1310 and 1266 cm^{-1} bands mirror the model data. Only the H−D exchange effect on the 1107 cm^{-1} trough does not mirror the L-histidine model data: in the imidazole minus imidazolate difference spectra of L-histidine, the effect of H−D exchange was very small, whereas it appears to cause almost complete loss of the trough in the ISP spectra in both cases. However, the imidazole form of L-histidine in solution consists of a mixture of forms in which either N_π or N_τ is protonated. This gives rise to the doublet at 1087 (N_τ-protonated) and 1105 cm^{-1}

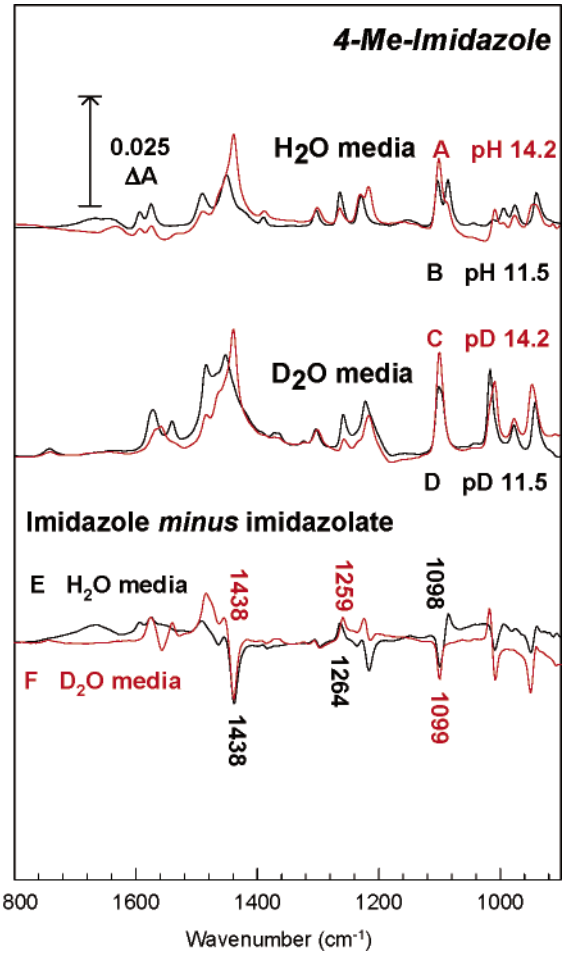

FIGURE 5: IR spectra of imidazole and imidazolate forms of 4-methylimidazole in aqueous media. Absolute ATR-FTIR spectra of 4-methylimidazole (500 mM) are shown at pH 14.2 (A, red) and pH 11.5 (B, black) in H_2O media and pD 14.2 (C, red) and pD 11.5 (D, black) in D_2O media. Solvent contributions to the spectra have been subtracted. The imidazole minus imidazolate difference spectra were calculated in H_2O as spectrum E (B minus A, black) and in D_2O as spectrum F (C minus A, red).

(N_π-protonated) (*65*, *66*) in the absolute imidazole spectrum in Figure 6. In the ISP, however, the histidine residues (H141/161 in bovine and H135/156 in *Rba. capsulatus*) are ligated to the [2Fe-2S] cluster via N_π atoms, and only a single band of N_τ-protonated imidazole is therefore predicted in the 1080−1100 cm^{-1} region. In contrast to N_π-protonated imidazole, the N_τ-protonated form is upshifted by 5−10 cm^{-1} after H−D exchange (*66*), shifting it close to the expected frequency of the H−D exchange insensitive imidazolate form. Hence, a loss of the trough in this region of the imidazole minus imidazolate form may be considered characteristic of the (relatively unusual) N_π-metal ligated histidine structure. This may also account for the fact that, while the 1266 cm^{-1} band in the ISP difference spectra in H_2O (Figures 2C,D and 3E,F) is shifted in D_2O to one distinct peak at 1257 cm^{-1}, the equivalent band in model L-histidine at 1262 cm^{-1} in H_2O appears to give two bands in D_2O (Figure 6E,F). It is therefore concluded that the 1447 cm^{-1} trough in the ISP redox difference spectra, together with the 1310, 1266, and 1107 cm^{-1} changes, represents the loss of the imidazolate form of one or both of the N_π-ligated imidazole histidine ligands to the [2Fe-2S] center, being in the imidazolate form in the oxidized protein above pH 7.6

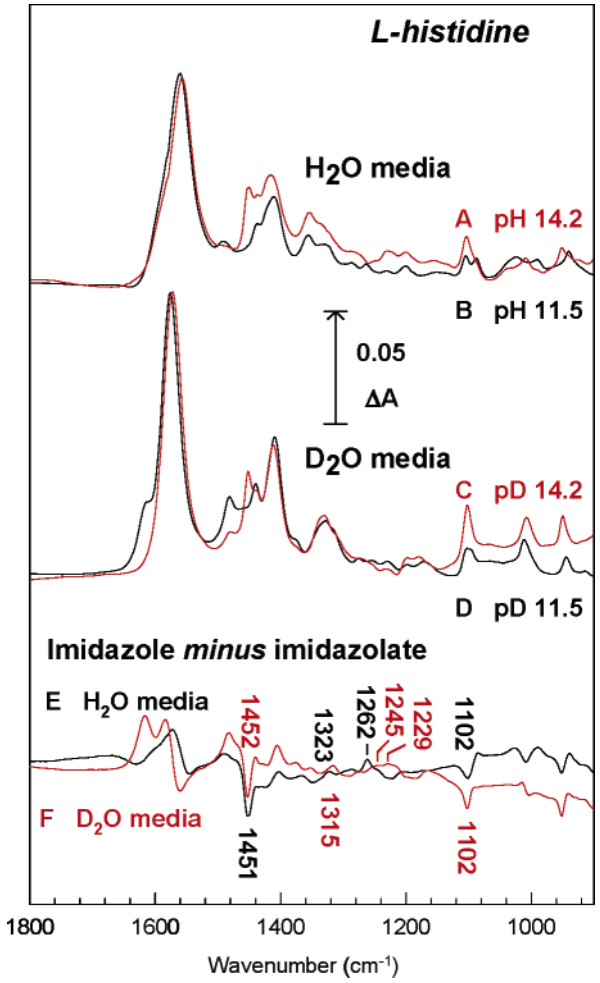

FIGURE 6: IR spectra of imidazole and imidazolate forms of L-histidine in aqueous media. Absolute ATR-FTIR spectra of L-histidine (500 mM) are shown at pH 14.2 (A, red) and pH 11.5 (B, black) in H_2O media and at pD 14.2 (C, red) and pD 11.5 (D, black) in D_2O media. The solvent contributions to the spectra have been subtracted. The imidazole minus imidazolate difference spectra were calculated in H_2O as spectrum E (B minus A, black) and in D_2O as spectrum F (C minus A, red).

and receiving a redox-linked proton when the ISP becomes reduced.

It should be noted that these assignments for the metal-bound histidine of the ISP have been made by comparison with IR data on free histidine and 4-methylimidazole, rather than with metal-bound forms, and questions about the expected extent of change due to metal ligation remain. Unfortunately, no IR measurements have been reported on metal-bound imidazolate models. However, calculations of Hasegawa et al. (*64*) on the imidazolate forms of zinc-bound 4-methylimidazole indicate that the same major bands persist, and in a recent paper, Dupeyrat et al. (*67*) reported similar band patterns for the free and cupric-bound forms of neutral 4-methylimidazole. Hence, we conclude provisionally that metal ligation has a limited effect on the imidazolate bands. This point will be investigated directly with future measurements of appropriate model compounds.

By inclusion of a marker with a known extinction coefficient when measuring the L-histidine spectra, it is possible to calculate the extinction coefficients of the component bands even in ATR measurement mode, since the depth of penetration of the evanescent wave, and therefore the effective path length, is inversely proportional to frequency (*28*). We used 10 mM potassium ferrocyanide for this purpose since it has a single noninterfering band at 2038 cm^{-1} with an extinction coefficient (determined by transmission IR separately) of 4140 M^{-1} cm^{-1}. This was used to calculate the effective path length at specific frequencies, allowing calculation of the extinction coefficients of features of the L-histidine imidazolate minus imidazole difference spectra by measurement at several pH values and using the published p*K* of 14.37 (*68*). This gave an extinction coefficient of −260 M^{-1} cm^{-1} for the frequency pair 1451 of 1470 cm^{-1}. This is a fairly strong intensity with a reasonably narrow half-bandwidth of 11 cm^{-1}. Furthermore, it is a frequency outside the amide I and II envelopes and one at which few other amino acids have strong bands. Hence, it should be valuable as a relatively specific marker band for the detection of imidazolate histidine in catalytic mechanisms of other enzymes. It might be noted that such a band was not detected in a detailed Raman study of an unusual imidazolate histidine in the active site of superoxide dismutase (*69*), and this is because the vibration does not give rise to a strong Raman band (*64*), presumably because of unfavorable selection rules. In the data of Figure 3, the 1447/1451 cm^{-1} trough bandwidth of 16−17 cm^{-1} is significantly broader than that of L-histidine in solution and shows some evidence of a small frequency shift with pH. This, together with the fact that the band appears to titrate over a broad pH range makes it likely that both histidine ligands are undergoing the imidazolate to imidazole transition, hence accounting for the two redox-linked p*K* values that have been detected by redox potentiometry (*49*, *57*). However, from the point of view of mechanism, it is likely that only the lower-p*K* histidine is mechanistically significant, and this certainly undergoes the redox-linked protonation. As has been widely suggested, N_τ of this histidine (H161 in bovine and H156 in *Rba. capsulatus*) should form the hydrogen bond acceptor for the incoming quinol substrate and can do so only in its imidazolate form. However, the observed p*K* of the quinol oxidation activity of the Q_o site is around pH 6.5 [bovine (*70*)] or pH 7 [bacterial (*23*, *57*)], becoming inactive below the p*K*. Hence, the operative p*K* of the histidine ligand in the catalytically active enzyme−substrate complex is most likely to be shifted from 7.6 to these lower values due to the hydrogen bonding with the quinol substrate, and it is this interaction and its p*K* that provide the primary physiological pH control of *bc* (and photosynthetic *bf*) complex quinol oxidation rates.

ACKNOWLEDGMENT

We thank Dr. Fevzi Daldal for a generous gift of the *Rba. capsulatus* strain containing the M183K mutation and Mr. Santiago Garcia and Ms. Vasanti Amin for expert technical support.

REFERENCES

1. Xia, D., Yu, C.-A., Hoeon, K., Xia, J. Z., Kachurin, A. M., Zhang, L., and Deisenhofer, J. (1997) Crystal structure of the cytochrome bc_1 complex from bovine heart mitochondria, *Science 277*, 60−66.
2. Zhang, Z., Huang, L., Shulmeister, V. M., Chi, Y.-I., Kim, K. K., Hung, L.-W., Crofts, A. R., Berry, E. A., and Kim, S.-H. (1998) Electron transfer by domain movement in cytochrome bc_1, *Nature 392*, 677−684.

3. Iwata, S., Lee, J. W., Okada, K., Lee, J. K., Iwata, M., Rasmussen, B., Link, T. A., Ramaswamy, S., and Jap, B. K. (1998) Complete structure of the 11-subunit bovine mitochondrial bc_1 complex, *Science 281*, 64−71.
4. Hunte, C., Koepke, J., Lange, C., Rossmanith, T., and Michel, H. (2000) Structure at 2.3 Å resolution of the cytochrome bc_1 complex from the yeast *Saccharomyces cerevisiae* co-crystallized with antibody Fv fragment, *Struct. Folding Des. 8*, 669−684.
5. Berry, E. A., Huang, L.-S., Saechao, L. K., Pon, N. G., Valkova-Valchanova, M., and Daldal, F. (2004) X-ray structure of *Rhodobacter capsulatus* cytochrome bc_1: Comparison with its mitochondrial and chloroplast counterparts, *Photosynth. Res. 81*, 251−275.
6. Kurisu, G., Zhang, H., Smith, J. L., and Cramer, W. A. (2003) Structure of the cytochrome b_6f complex of oxygenic photosynthesis: Tuning the cavity, *Science 302*, 1009−1014.
7. Stroebel, D., Choquet, Y., Popot, J.-L., and Picot, D. (2003) An atypical haem in the cytochrome b_6f complex, *Nature 426*, 413−418.
8. Mitchell, P. (1976) Possible molecular mechanisms of the protonmotive function of cytochrome systems, *J. Theor. Biol. 62*, 327−367.
9. Darrouzet, E., Moser, C. C., Dutton, P. L., and Daldal, F. (2001) Large scale domain movement in cytochrome bc_1: A new device for electron transfer in proteins, *Trends Biochem. Sci. 26*, 445−451.
10. Crofts, A. R., Guergova-Kuras, M., Huang, L.-S., Kuras, R., Zhang, Z., and Berry, E. A. (1999) Mechanism of ubiquinol oxidation by the bc_1 complex: Role of the iron sulfur protein and its mobility, *Biochemistry 38*, 15791−15806.
11. Crofts, A. R., Hong, S., Zhang, Z., and Berry, E. A. (1999) Physiochemical aspects of the movement of the Rieske iron sulfur protein during quinol oxidation by the bc_1 complex from mitochondria and photosynthetic bacteria, *Biochemistry 38*, 15827−15839.
12. Darrouzet, E., Valkova-Valchanova, M., and Daldal, F. (2002) The [2Fe-2S] cluster as an indicator of the iron−sulfur subunit position in the ubihydroquinone oxidation site of the cytochrome bc_1 complex, *J. Biol. Chem. 277*, 3464−3470.
13. Crofts, A. R., Barquera, B., Gennis, R. B., Kuras, R., Guergova-Kuras, M., and Berry, E. A. (1999) Mechanism of ubiquinol oxidation by the bc_1 complex: Different domains of the quinol binding pocket and their role in the mechanism and binding of inhibitors, *Biochemistry 38*, 15807−15826.
14. Ding, H., Robertson, D. E., Daldal, F., and Dutton, P. L. (1992) Cytochrome bc_1 complex [2Fe-2S] cluster and its interaction with ubiquinone and ubihydroquinone at the Q_o site: A double-occupancy Q_o site model, *Biochemistry 31*, 3144−3158.
15. Brandt, U., Schägger, H., and von Jagow, G. (1988) Characterisation of binding of the methoxyacrylate inhibitors to mitochondrial cytochrome *c* reductase, *Eur. J. Biochem. 173*, 499−506.
16. Bartoschek, S., Johansson, M., Geierstanger, B. H., Okun, J. G., Lancaster, C. R. D., Humpfer, E., Yu, L., Yu, C.-A., Griesinger, C., and Brandt, U. (2001) Three molecules of ubiquinone bind specifically to mitochondrial cytochrome bc_1 complex, *J. Biol. Chem. 276*, 35231−35234.
17. Brandt, U. (1996) Bifurcated ubihydroquinone-oxidation in the cytochrome bc_1 complex by proton-gated charge-transfer, *FEBS Lett. 387*, 1−6.
18. Brandt, U. (1998) The chemistry and mechanics of ubihydroquinone oxidation at center P (Q_o) of the cytochrome bc_1 complex, *Biochim. Biophys. Acta 1365*, 261−268.
19. Jünemann, S., Heathcote, P., and Rich, P. R. (1998) On the mechanism of quinol oxidation in the bc_1 complex, *J. Biol. Chem. 273*, 21603−21607.
20. Link, T. A. (1997) The role of the 'Rieske' iron sulfur protein in the hydroquinone oxidation (Q_P) site of the cytochrome bc_1 complex, *FEBS Lett. 412*, 257−264.
21. Trumpower, B. L., and Gennis, R. B. (1994) Energy transduction by cytochrome complexes in mitochondrial and bacterial respiration: The enzymology of coupling electron transfer reactions to transmembrane proton translocation, *Annu. Rev. Biochem. 63*, 675−716.
22. Snyder, C. H., Gutiérrez-Circlos, E.-B., and Trumpower, B. L. (2000) Evidence for a concerted mechanism of ubiquinol oxidation by the cytochrome bc_1 complex, *J. Biol. Chem. 275*, 13535−13541.
23. Osyczka, A., Moser, C. C., Daldal, F., and Dutton, P. L. (2004) Reversible redox energy coupling in electron transfer chains, *Nature 427*, 607−612.
24. Berry, E. A., and Huang, L.-S. (2003) Observations concerning the quinol oxidation site of the cytochrome bc_1 complex, *FEBS Lett. 555*, 13−20.
25. Klishin, S. S., Junge, W., and Mulkidjanian, A. Y. (2002) Flash-induced turnover of the cytochrome bc_1 complex in chromatophores of *Rhodobacter capsulatus*: Binding of Zn^{2+} decelerates likewise the oxidation of cytochrome *b*, the reduction of cytochrome c_1 and the voltage generation, *Biochim. Biophys. Acta 1553*, 177−182.
26. Rich, P. R. (2004) The quinone chemistry of *bc* complexes, *Biochim. Biophys. Acta 1658*, 165−171.
27. Crofts, A. R. (2004) The cytochrome bc_1 complex: Function in the context of structure, *Annu. Rev. Physiol. 66*, 689−733.
28. Goormaghtigh, E., Raussens, V., and Ruysschaert, J.-M. (1999) Attenuated total reflection infrared spectroscopy of proteins and lipids in biological membranes, *Biochim. Biophys. Acta 1422*, 105−185.
29. Zscherp, C., Schlesinger, R., Tittor, J., Oesterhelt, D., and Heberle, J. (1999) In situ determinatin of transient pK_a changes of internal amino acids of bacteriorhodopsin by using time-resolved atenuated total reflection Fourier transform infrared spectroscopy, *Proc. Natl. Acad. Sci. U.S.A. 96*, 5498−5503.
30. Baenziger, J. E., Miller, K. W., and Rothschild, K. J. (1993) Fourier transform infrared difference spectroscopy of the nicotinic acetylcholine receptor: Evidence for specific protein structural changes upon desensitization, *Biochemistry 32*, 5448−5454.
31. Mäntele, W., Nabedryk, E., Tavitian, B. A., Kreutz, W., and Breton, J. (1985) Light-induced Fourier transform infrared (FTIR) spectroscopic investigations of the primary oxidation in bacterial photosynthesis, *FEBS Lett. 187*, 227−232.
32. Tabitian, B. A., Nabedryk, E., Mäntele, W., and Breton, J. (1986) Light-induced Fourier transform infrared (FTIR) spectroscopic investigations of primary reactions in photosystem I and photosystem II, *FEBS Lett. 201*, 151−157.
33. Iwaki, M., Andrianambinintsoa, S., Rich, P. R., and Breton, J. (2002) Attenuated total reflection Fourier transform infrared spectroscopy of redox transitions in photosynthetic reaction centers: Comparison of perfusion- and light-induced difference spectra, *Spectrochim. Acta A58*, 1523−1533.
34. Hellwig, P., Rost, B., Kaiser, U., Ostermeier, C., Michel, H., and Mäntele, W. (1996) Carboxyl group protonation upon reduction of the *Paracoccus denitrificans* cytochrome *c* oxidase: Direct evidence by FTIR spectroscopy, *FEBS Lett. 385*, 53−57.
35. Hellwig, P., Behr, J., Ostermeier, C., Richter, O.-M. H., Pfitzner, U., Odenwald, A., Ludwig, B., Michel, H., and Mäntele, W. (1998) Involvement of glutamic acid 278 in the redox reaction of the cytochrome *c* oxidase from *Paracoccus denitrificans* investigated by FTIR spectroscopy, *Biochemistry 37*, 7390−7399.
36. Lübben, M., and Gerwert, K. (1996) Redox FTIR difference spectroscopy using caged electrons reveals contributions of carboxyl groups to the catalytic mechanism of haem-copper oxidases, *FEBS Lett. 397*, 303−307.
37. Yamazaki, Y., Kandori, H., and Mogi, T. (1999) Effects of subunit I mutations on redox-linked conformational changes of the *Escherichia coli bo*-type ubiquinol oxidase revealed by Fourier-transform infrared spectroscopy, *J. Biochem. 126*, 194−199.
38. Lübben, M., Prutsch, A., Mamat, B., and Gerwert, K. (1999) Electron transfer induces side-chain conformational changes of glutamate-286 from cytochrome bo_3, *Biochemistry 38*, 2048−2056.
39. Hellwig, P., Soulimane, T., Buse, G., and Mäntele, W. (1999) Similarities and dissimilarities in the structure−function relation between the cytochrome *c* oxidase from bovine heart and from *Paracoccus denitrificans* as revealed by FT-IR difference spectroscopy, *FEBS Lett. 458*, 83−86.
40. Rich, P. R., and Breton, J. (2002) Attenuated total reflection Fourier transform infrared studies of redox changes in bovine cytochrome *c* oxidase: Resolution of the redox Fourier transform infrared difference spectrum of heme a_3, *Biochemistry 41*, 967−973.
41. Nyquist, R. M., Heitbrink, D., Bolwien, C., Wells, T. A., Gennis, R., and Heberle, J. (2001) Perfusion-induced redox differences in cytochrome *c* oxidase: ATR/FT-IR spectroscopy, *FEBS Lett. 505*, 63−67.
42. Iwaki, M., Breton, J., and Rich, P. R. (2002) ATR-FTIR difference spectroscopy of the P_M intermediate of bovine cytochrome *c* oxidase, *Biochim. Biophys. Acta 1555*, 116−121.

43. Hellwig, P., Scheide, D., Bungert, S., Mäntele, W., and Friedrich, T. (2000) FT-IR spectroscopic characterization of NADH:ubiquinone oxidoreductase (complex I) from *Esherichia coli*: Oxidation of FeS cluster N2 is coupled with the protonation of an aspartate or glutamate side chain, *Biochemistry 39*, 10884−10891.
44. Baymann, F., Robertson, D. E., Dutton, P. L., and Mäntele, W. (1999) Electrochemical and spectroscopic investigations of the cytochrome bc_1 complex from *Rhodobacter capsulatus*, *Biochemistry 38*, 13188−13199.
45. Ritter, M., Anderka, O., Ludwig, B., Mäntele, W., and Hellwig, P. (2003) Electrochemical and FTIR spectroscopic characterization of the cytochrome bc_1 complex from *Paracoccus denitrificans*: Evidence for protonation reactions coupled to quinone binding, *Biochemistry 42*, 12391−12399.
46. Iwaki, M., Giotta, L., Akinsiku, A. O., Schägger, H., Fisher, N., Breton, J., and Rich, P. R. (2003) Redox-induced transitions in bovine cytochrome bc_1 complex studied by perfusion-induced ATR-FTIR spectroscopy, *Biochemistry 42*, 11109−11119.
47. Iwaki, M., Osyczka, A., Moser, C. C., Dutton, P. L., and Rich, P. R. (2004) ATR-FTIR spectroscopy studies of ion-sulfur protein and cytochrome c_1 in the *Rhodobacter capsulatus* cytochrome bc_1 complex, *Biochemistry 43*, 9477−9486.
48. Robertson, D. E., Daldal, F., and Dutton, P. L. (1990) Mutants of ubiquinol cyt c_2 oxidoreductase resistant to Qo site inhibitors: Consequences for ubiquinone and ubiquinol affinity and catalysis, *Biochemistry 29*, 11249−11260.
49. Link, T. A., Hagen, W. R., Pierik, A. J., Assmann, C., and von Jagow, G. (1992) Determination of the redox properties of the Rieske [2Fe-2S] cluster of bovine heart bc_1 complex by direct electrochemistry of a water-soluble fragment, *Eur. J. Biochem. 208*, 685−691.
50. Leggate, E. J., Bill, E., Essigke, T., Ullmann, G. M., and Hirst, J. (2004) Formation and characterization of an all-ferrous Rieske cluster and stabilization of the $[2Fe\text{-}2S]^0$ core by protonation, *Proc. Natl. Acad. Sci. U.S.A. 101*, 10913−10918.
51. Robertson, D. E., Ding, H., Chelminski, P. R., Slaughter, C., Hsu, J., Moomaw, C., Tokito, M., Daldal, F., and Dutton, P. L. (1993) Hydroubiquinone-cytochrome c_2 oxidoreductase from *Rhodobacter capsulatus*: Definition of a minimal, functional isolated preparation, *Biochemistry 32*, 1310−1317.
52. Darrouzet, E., Mandaci, S., Li, J., Qin, H., Knaff, D. B., and Daldal, F. (1999) Substitution of the sixth axial ligand of *Rhodobacter capsulatus* cytochrome c_1 heme yields novel cytochrome c_1 variants with unusual properties, *Biochemistry 38*, 7908−7917.
53. Leggate, E. J. (2003) Coupled electron and proton transfer at iron-sulphur clusters in the electron transport chain, Ph.D. Thesis, University of Cambridge, Cambridge, U.K.
54. Glasoe, P. K., and Long, F. A. (1960) Use of glass electrodes to measure acidities in deuterium oxide, *J. Phys. Chem. 64*, 188−190.
55. Rath, P., DeGrip, W. J., and Rothschild, K. J. (1998) Photoactivation of rhodopsin causes an increased hydrogen−deuterium exchange of buried peptide groups ,*Biophys. J. 74*, 192−198.
56. Arrondo, J. L. R., Muga, A., Castresana, J., and Goñi, F. M. (1993) Quantitative studies of the structure of proteins in solution by Fourier transform infrared spectroscopy, *Prog. Biophys. Mol. Biol. 59*, 23−56.
57. Guergova-Kuras, M., Kuras, R., Ugulava, N., Hadad, I., and Crofts, A. R. (2000) Specific mutagenesis of the Rieske iron−sulfur protein in *Rhodobacter sphaeroides* shows that both the thermodynamic gradient and the p*K* of the oxidized form determine the rate of quinol oxidation by the bc_1 complex, *Biochemistry 39*, 7436−7444.
58. Iwata, S., Saynovits, M., Link, T. A., and Michel, H. (1996) Structure of a water soluble fragment of the "Rieske" iron−sulfur protein of the bovine heart mitochondrial bc_1 complex determined by MAD phasing at 1.5 Å resolution, *Structure 4*, 567−579.
59. Zu, Y., Couture, M. M. J., Kolling, D. R. J., Crofts, A. R., Eltis, L. D., Fee, J. A., and Hirst, J. (2003) Reduction potential of Rieske clusters: Importance of the coupling between oxidation state and histidine protonation state, *Biochemisry 42*, 12400−12408.
60. Iwasaki, T., Kounosu, A., Kolling, D. R. J., Crofts, A. R., Dikanov, S. A., Jin, A., Imai, T., and Urushiyama, A. (2004) Characterization of the pH-dependent resonance Raman transitions of archaeal and bacterial Rieske [2Fe-2S] proteins, *J. Am. Chem. Soc. 126*, 4788−4789.
61. Kuila, D., and Fee, J. A. (1986) Evidence for a redox-linked ionizable group associated with the [2Fe-2S] cluster of *Thermus* Rieske protein, *J. Biol. Chem. 261*, 2768−2771.
62. Kuila, D., Schoonover, J. R., Dyer, R. B., Batie, C. J., Ballou, D. P., Fee, J. A., and Woodruff, W. H. (1993) Resonance Raman studies of Rieske-type proteins, *Biochim. Biophys. Acta 1140*, 175−183.
63. Samoiloca, R. I., Kolling, D., Uzawa, T., Iwasaki, T., Crofts, A. R., and Dikanov, S. A. (2002) The interaction of the Rieske iron−sulfur protein with occupants of the Q_0-site of the bc_1 complex, probed by electron spin−echo envelope modulation, *J. Biol. Chem. 277*, 4605−4608.
64. Hasegawa, K., Ono, T.-A., and Noguchi, T. (2000) Vibrational spectra and ab initio DFT calculations of 4-methylimidazole and its different protonation forms: Infrared and Raman markers of the protonation state of a histidine side chain, *J. Phys. Chem. B 104*, 4253−4265.
65. Hasegawa, K., Ono, T.-A., and Noguchi, T. (2002) Ab initio density functional theory calculations and vibrational analysis of zinc-bound 4-methilimidazole as a model of a histidine ligand in metalloenzymes, *J. Phys. Chem. A 106*, 3377−3390.
66. Noguchi, T., Inoue, Y., and Tang, X.-S. (1999) Structure of a histidine ligand in the photosynthetic oxygen-evolving complex as studied by light-induced Fourier transform infrared difference spectroscopy, *Biochemistry 38*, 10187−10195.
67. Dupeyat, F., Vidaud, C., Lorphelin, A., and Berthomieu, C. (2004) Long distance charge redistribution upon Cu,Zn-superoxide dismutase reduction, *J. Biol. Chem. 279*, 48091−48101.
68. Yagil, G. (1967) The proton dissociation constant of pyrrole, indole and related compounds, *Tetrahedron 23*, 2855−2861.
69. Wang, D., Zhao, X., Vargek, M., and Spiro, T. G. (2000) Metal-bound histidine modes in UV resonance Raman spectra of Cu,Zn superoxide dismutase, *J. Am. Chem. Soc. 122*, 2193−2199.
70. Rich, P. R. (1984) Electron and proton transfers through quinones and cytochrome *bc* complexes, *Biochim. Biophys. Acta 768*, 53−79.

BI047533V